Monthly Notices
of the
ROYAL ASTRONOMICAL SOCIETY

MNRAS **440,** 1649–1661 (2014) doi:10.1093/mnras/stu326
Advance Access publication 2014 March 25

ExoMol line lists – IV. The rotation–vibration spectrum of methane up to 1500 K

Sergei N. Yurchenko★ and Jonathan Tennyson★

Department of Physics and Astronomy, University College London, London WC1E 6BT, UK

Accepted 2014 February 17. Received 2014 February 9; in original form 2013 December 22

ABSTRACT

A new hot line list is calculated for $^{12}CH_4$ in its ground electronic state. This line list, called 10to10, contains 9.8 billion transitions and should be complete for temperatures up to 1500 K. It covers the wavelengths longer than 1 μm and includes all transitions to upper states with energies below $hc \cdot 18\,000$ cm^{-1} and rotational excitation up to $J = 39$. The line list is computed using the eigenvalues and eigenfunctions of CH_4 obtained by variational solution of the Schrödinger equation for the rotation–vibration motion of nuclei employing program TROVE and a new 'spectroscopic' potential energy surface (PES) obtained by refining an ab initio PES (CCSD(T)-F12c/aug-cc-pVQZ) through least-squares fitting to the experimentally derived energies with $J = 0-4$ and a previously reported ab initio dipole moment surface (CCSD(T)-F12c/aug-cc-pVTZ). Detailed comparisons with other available sources of methane transitions including HITRAN, experimental compilations and other theoretical line lists show that these sources lack transitions both higher temperatures and near-infrared wavelengths. The 10to10 line list is suitable for modelling atmospheres of cool stars and exoplanets. It is available from the CDS data base as well as at www.exomol.com.

Key words: molecular data – opacity – astronomical data bases: miscellaneous – planets and satellites: atmospheres – stars: low-mass.

1 INTRODUCTION

Methane plays an important role in atmospheric and astrophysical chemistry. Its rotation–vibration spectrum is of key importance for models of the atmospheres of bodies ranging from Titan to brown dwarfs. Any temperature-dependent model of the methane spectrum requires comprehensive information on the associated transition intensities.

Methane was detected in the exoplanet HD189733b by Swain, Vasisht & Tinetti (2008) and further studied using ground-based observations by Swain et al. (2010). However, the abundance of exoplanetary methane has sometimes proved controversial (Stevenson et al. 2010; Beaulieu et al. 2011). On earth methane is an important global warming species (Rhoderick & Dorko 2004) and a biosignature (Sagan et al. 1993); spectra of hot methane are also required for a variety of terrestrial applications including the study of combustion (Jourdanneau et al. 2007) and sensing (Wolff et al. 2013). Methane has been detected on Mars (Atreya, Mahaffy & Wong 2007) although these observations have not always proved repeatable (Krasnopolsky 2012). On Earth-like planets outside our Solar system, whose spectra of course have yet to be observed, methane has long been thought of as a key potential biosignature (Sagan et al. 1993; Atreya et al. 2007).

Methane is well known in cool carbon stars and brown dwarfs (Bernath 2009); indeed, T-dwarfs are often referred to as methane dwarfs (Lucas et al. 2010). However, modelling methane in these objects with available laboratory data has often proved difficult (Geballe et al. 1996; Bailey & Kedziora-Chudczer 2012). Similarly, hot methane emissions were observed in aftermath of the collision of comet Shoemaker–Levy 9 with Jupiter (Maillard et al. 1995; Dinelli et al. 1997).

Given the importance of methane spectra, a growing number of $^{12}CH_4$ rotation–vibration line lists are available. The standard for atmospheric spectroscopy is HITRAN and the recently released 2012 edition (Rothman et al. 2013) contains a thorough update for methane as detailed by Brown et al. (2013). However, HITRAN is designed for work at Earth atmosphere temperatures and its companion, high-temperature data base HITEMP (Rothman et al. 2010) does not include methane. Other sources include a high-temperature line list computed by Warmbier et al. (2009), the MeCaSDa spectroscopic data base containing largely empirical line list (Ba et al. 2013) and a partial experimental line list WKMC constructed by Campargue et al. (2013). Finally, high-temperature experimental line lists are available due to Nassar & Bernath (2003), Thiévin et al. (2008) and Hargreaves et al. (2012). Measured methane cross-sections are also provided in the PNNL data base (Sharpe et al.

★ E-mail: s.yurchenko@ucl.ac.uk (SNY); j.tennyson@ucl.ac.uk (JT)

2004). As discussed below, none of these compilations are complete at the elevated temperatures considered in this work.

Recently, we (Tennyson & Yurchenko 2012) started the ExoMol project which aims to generate a comprehensive library of line list for all molecules likely to be important for modelling atmospheres of exoplanets and cool stars. Here, we employ the variational program TROVE (Yurchenko, Thiel & Jensen 2007) to construct a synthetic line list for $^{12}CH_4$ in its ground electronic state. To this end, the Schrödinger equation for the rotation–vibration motion of nuclei is solved to obtain eigenvalues (ro-vibrational energies) and eigenfunctions (nuclear motion wavefunctions). The latter are necessary for ro-vibrational averaging of the dipole moment of the molecule and thus to compute the transitional probabilities, usually expressed in terms of the Einstein coefficients or line strengths. Such calculations are based on the use of a potential energy surface (PES) and dipole moment surfaces (DMSs).

There have been many quantum-chemical studies of methane. We will concentrate on those aimed at producing comprehensive rotation–vibration line lists. Oyanagi et al. (2006) presented ab initio PES calculations based at the CCSD(T)/cc-pVTZ and MP2/cc-pVTZ level of theory. Warmbier et al. (2009) used RCCSD(T)/aug-cc-pVTZ theory to compute a hot line list containing 1.4 million. Nikitin, Rey & Tyuterev (2011) constructed a PES which they showed to provide accurate (within 1 cm^{-1}) vibrational energies of CH_4. Nikitin, Rey & Tyuterev (2013) recently presented new ab initio, methane DMSs based on the CCSD(T)/cc-pCVQZ level of theory. Rey, Nikitin & Tyuterev (2013a,b) employed these PES and DMSs to simulate the room temperature infrared (IR) absorption spectrum of CH_4. Comparison with laboratory experiments showed that their predicted intensities agreed well indicating the high quality of the underlying ab initio DMSs. Other recent studies on methane include those by Schwenke & Partridge (2001) and Schwenke (2002), Wang & Carrington (2013) and Mielke, Chakraborty & Truhlar (2013).

In this work, we present a new 'spectroscopic' PES obtained by fitting an ab initio PES from Yurchenko et al. (2013) to the experimental energies of CH_4 with $J = 0{-}4$. The ab initio DMS of Yurchenko et al. (2013), obtained at the CCSD(T)/aug-cc-pVTZ level of theory, is used to compute the line strengths.

The paper is structured as follows. The following section introduces the PES and DMSs, as well as the quantum number scheme used to label the ro-vibrational states of CH_4 (also discussed in detail in the appendix). Section 3 describes the variational procedure used to solve the Schrödinger equation. The intensity calculations and the line list generated are detailed in Section 4. The evaluation of the new line list and comparisons against different empirical and theoretical line lists are given in Section 6. Some conclusions are offered in Section 7.

2 BACKGROUND TO THE CALCULATION

In the following, CH_4 and methane will refer to the main isotopologue $^{12}CH_4$ of methane unless specified.

Methane is a symmetric five atomic molecule characterized by nine vibrational degrees of freedom with a vanishing permanent dipole moment. It is a very high-symmetry molecule of the $\mathcal{T}_d(M)$ symmetry group containing a number of degenerate modes. As discussed in our recent work on ammonia (Down et al. 2013), this situation means that some care has to be taken in selecting an appropriate set of quantum numbers. Below, we specify our chosen quantum numbers for CH_4; reasons for this choice are given in the appendix.

Table 1. Vibrational modes of methane.

Mode	Symmetry	Type
1	A_1	Symmetric stretch
2	E	Asymmetric bend
3	F_1	Asymmetric stretch
4	F_2	Asymmetric bend

Table 2. The classification of the multiplicity index M_i ($i = 3, 4$, $M_i \leq L_i$) by symmetry ($n = 1, 2, 3, \ldots$).

Symmetry	M
A_1	$0 + 12\,n$
A_2	$6 + 12\,n$
E	$2 + 6\,n$
F_1	$3 + 4\,n$
F_2	$1 + 4\,n$

The symmetry properties of methane spectra have been carefully considered by Hougen (2001), and we used this work as our starting point. Using the Molecular Symmetry group (Bunker & Jensen 2004), the total ro-vibrational states of CH_4 have total symmetry, Γ_{tot}, either A_1, A_2, E, F_1 or F_2. Considering the H nuclear spin, the nuclear statistical weight, g_{ns}, takes the value 5, 5, 2, 3, and 3 for each symmetry, respectively. The electric dipole transitions obey the following symmetry-determined selection rules:

$$A_1 \leftrightarrow A_2\ ,\ E \leftrightarrow E\ ,\ F_1 \leftrightarrow F_2 \tag{1}$$

with the standard rotational angular momentum, $\boldsymbol{J}$, selection rules:

$$J \leftrightarrow J \pm 1\ \ ,\ J' + J'' \neq 0. \tag{2}$$

Our set of quantum numbers consists of the following 15 labels:

$$\begin{aligned} \mathrm{QN} = {} & \Gamma_{tot}, J, K, \Gamma_{rot}, n_1, n_2, L_2, n_3, L_3, \\ & M_3, n_4, L_4, M_4, \Gamma_{vib}, N_{J,\Gamma_{tot}}, \end{aligned} \tag{3}$$

where Γ_{rot} and Γ_{vib} are the symmetries of the rotational and vibrational wavefunction, respectively, $K = 0, \ldots, J-1, J$ is the absolute value of the projection of the rotational angular momentum of J on to the body-fixed z-axis, and n_1, n_2, L_2, n_3, L_3, M_3, n_4, L_4, M_4 are the normal mode vibrational quantum numbers (see the mode designation in Table 1). We follow Down et al. (2013) and use the only the absolute values of the vibrational angular momentum quantum numbers $L_i = n_i, n_i - 2, \ldots, 0(1)$. $M_i \leq L_i$ is a multiplicity index used to count states within a given n_i, L_i set (see Boudon, Rey & Loëte 2006) and indicate the symmetry according to Table 2. Finally, as it is often not possible to uniquely define CH_4 quantum numbers, a counting number $N_{J,\Gamma_{tot}}$ is also included. This number runs over states of a given total symmetry and J.

To calculate the ro-vibrational energies in the Born–Oppenheimer approximations, a PES is required. In this work, we use a new 'spectroscopic' PES obtained by refining an ab initio PES through fits to experimental ro-vibrational energies. To this end, a set of experimental term values with $J \leq 4$ was selected ranging up to 6100 cm^{-1} derived from frequencies collected in the HITRAN 2008 data base (Rothman et al. 2009). We recently produced a 'spectroscopic' CH_4 PES using a similar procedure by fitting an ab initio CCSD(T)-F12/aug-cc-pVQZ PES to the same set of experimentally derived energies (Yurchenko et al. 2013). Here, the 'spectroscopic' PES of

Yurchenko et al. (2013) was further refined. This was necessary because our refinement procedure, and therefore the resulting PES, is sensitive to the size of the basis set used in the variational calculations. The basis set employed here is smaller than that used by Yurchenko et al. (2013). The effect of the basis set reduction is estimated to range from 1 to 2 cm^{-1} for the fundamental term values and to up to 10–40 cm^{-1} above $hc \cdot 8000$ cm^{-1} for some highly excited deformational overtones. However, the prediction accuracy of the empirically obtained PES is as good as 0.01–1 cm^{-1}, at least for the vibrational states used in the fit (see below).

The resulting PES is given as Supplementary Material to this paper in the form of a FORTRAN 95 program. It should be noted, however, that this PES has an 'effective' character and guarantees to give accurate results only in conjunction with the same method and basis set used to produce it with. This obvious disadvantage is a result of the non-converged basis set used in TROVE, as well as the approximate character of the kinetic and potential energy expansions employed.

The fitting set of our 'experimentally derived' term values (cm^{-1}) was built from combination differences arising from the transition wavenumbers collected in HITRAN 2008. It should be noted that only a few of the term values were supported by more than one transition.

In our procedure, as described in detail by Yurchenko et al. (2011a), the refined PES is formulated as a correction to the original PES:

$$V = V_0 + \Delta V, \tag{4}$$

where both V_0 and ΔV are presented as expansion in terms of the internal coordinate displacements. At the first stage, the Schrödinger equations are solved for the initial potential V_0 to obtain the eigenfuncitons $\Psi^{(0)}_{J,\lambda}$ for a set of the rotational quantum numbers J. These eigenfunctions are then used as basis functions for solving the Schrödinger equations with the probe PES V during the fitting procedure. In this way, only the matrix elements $\langle \Psi_{J,\lambda} | \Delta V | \Psi_{J,\lambda'} \rangle$ are required when solving the corresponding the Schrödinger equations variationally. In order to guarantee a physically correct shape of the fitted PES, it was constrained to follow closely the shape of the starting ab initio PES of CH_4 by simultaneously fitting the refined potential parameters to the experimental energy levels and ab initio (Yurchenko et al. 2003). This procedure allowed us to vary all 268 potential parameters defining the PES in the fit despite the apparent shortage of the experimental energies. The accuracy achieved in this fit is illustrated in Fig. 1, where the absolute values of the obs. minus calc. residuals are shown. The total root-mean-square (rms) error for 317 term values used is 0.11 cm^{-1} with the major data points distributed between 0.01 and 0.1 cm^{-1}. It should be noted however that some of the transitions present in HITRAN 2008 (especially above 5 000 cm^{-1}) appeared to be relatively large outliers and therefore could not be included into our fitting set. This may indicate problems with our PES for the vibrational modes not properly sampled by out fitting set and/or assignment problems in HITRAN 2008. A comparison of the line positions computed using the refined PES (see below) also shows close agreement with the experimental data for $J > 4$, i.e. for the term values not included in the fit. This is to be expected since the extrapolation to high rotational excitations is known to work well, better than that for the vibrational excitations. The latter is difficult to quantify because of the limited amount of the reliable experimental data beyond 7 000 cm^{-1}. In the worst case which probably involves highly excited deformational modes, we expect our extrapolation accuracy to be no better than 10 cm^{-1} for levels lying above 10 000 cm^{-1}.

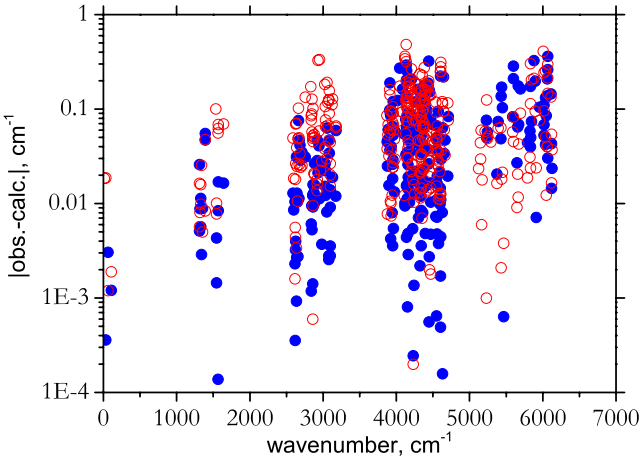

Figure 1. Residuals of CH_4 experimentally determined and calculated energy term values. Calculated using the refined PES before the shift of the vibrational band centres (red empty circles) and after (blue filled circles), see the text.

3 VARIATIONAL CALCULATIONS

The high symmetry of methane meant that a specially adapted version of TROVE had to be developed, details of which are given by Yurchenko et al. (2013). In TROVE, the basis set is built using the polyad number, which for CH_4 is given by

$$P = 2(v_1 + v_2 + v_3 + v_4) + v_5 + v_6 + v_7 + v_8 + v_9, \tag{5}$$

where v_i is a vibrational quantum number associated with the one-dimensional primitive basis function $\phi_{v_i}(\xi_i^\ell)$ ($i = 1, 2, 3, \ldots, 9$) and ξ_i^ℓ is an internal linearized coordinate, see below. In the conventional normal mode representation, this condition corresponds to

$$P = 2(n_1 + n_3) + n_2 + n_4. \tag{6}$$

The stretching basis functions $\phi_{v_i}(\xi_i^\ell)$ ($i = 1, -4$) were obtained by numerically solving a reduced, one-dimensional Hamiltonian problem using the Numerov–Cooley method. Harmonic oscillators were used for the bending basis functions $i = 5-9$. The basis set used was constructed from two major contributions, (i) all basis functions with the primitive quantum numbers satisfying $P \leq 10$ and (ii) stretching functions ranging up to $P = 20$ but with some high P-polyad ($P \geq 17$) stretching contributions that couple all modes together removed. This scheme is designed to reduce the basis set to the manageable size and at the same time to retain stretching basis functions with higher excitations than bending, giving preference to less-mixed modes. Our underlying assumption for this is that the stretching excitations carry the strongest transitions.

Following Yurchenko et al. (2013), the final contracted basis functions were obtained employing the $J = 0$ representation. In this representation, the $J = 0$ (vibrational) eigenfunctions are used together with symmetrized rigid rotor functions to construct the basis set functions for $J > 0$. For each J value, five symmetrized Hamiltonian matrices employing the $J = 0$ contraction scheme are computed and then diagonalized. In order to improve the prediction property of the refined potential of CH_4 (see Fig. 1) further, artificial band centre shifts were added to the $J = 0$ energies following the empirical basis set correction scheme (EBSC; Yurchenko et al. 2009). The result of the improvement can be seen in Fig. 1 as well.

In the TROVE approach, the Hamiltonian operator is represented as an expansion around a reference geometry taken here at the molecular equilibrium. The kinetic energy operator is expanded in

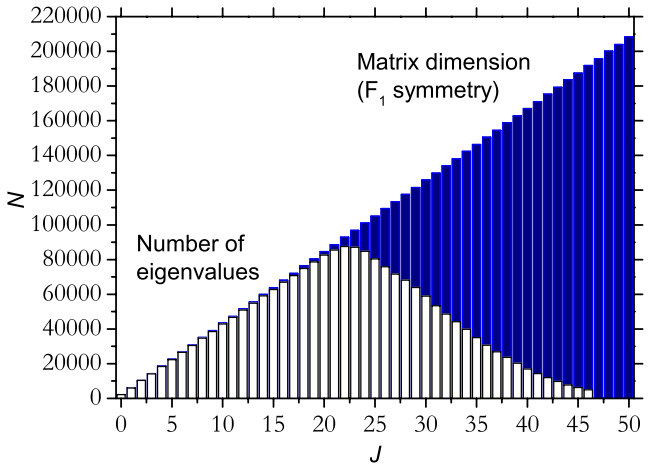

Figure 2. Size of the F_1-symmetry Hamiltonian matrix and the number of eigenvalues below 18000 cm^{-1} for each J.

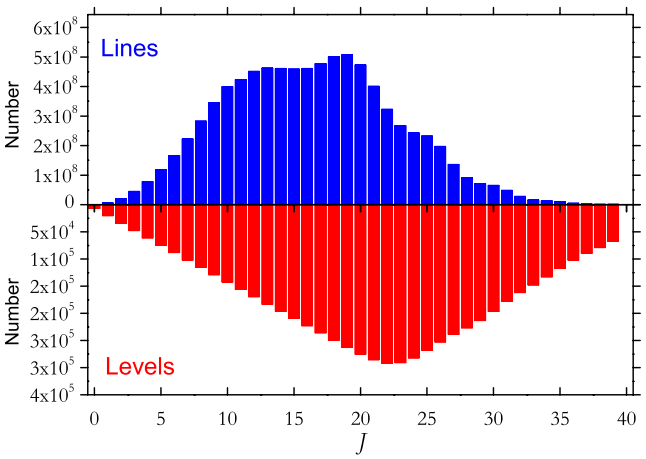

Figure 3. Number of energy levels and lines in the 10to10 line list per the rotational quantum number, J.

terms of the nine coordinates ξ_i^ℓ, which are linearized versions of the internal coordinates ξ_i ($i = 1, \ldots, 9$), see (Yurchenko et al. 2013); the potential energy function is expanded in terms of $1 - \exp(-a\xi_i^\ell)$ ($i = 1{-}4$) for the four stretching and ξ_j^ℓ ($j = 5{-}9$) for the five bending modes. The latter expansions were applied to the refined PES introduced above. The kinetic and potential energy parts were truncated at sixth- and eighth order, respectively.

The dimensions of the $J = 0$ basis sets used are 837, 585, 1418, 1916 and 2163 for the A_1, A_2, E, F_1 and F_2 symmetries, respectively. The (symmetrically adapted) ro-vibrational basis functions are represented by the (symmetrically reduced) direct product of $(2J + 1)$ rigid rotor wavefunctions and the $J = 0$ eigenfunctions. The size of the ro-vibrational basis set scales linearity with J as illustrated in Fig. 2, where the size of the F_{1x} matrix is shown for $J = 0, \ldots, 39$. The largest matrix to be diagonalized (F_{1x}, $J = 39$) has 163 034 × 163 034 elements. The dimension of the matrices of different symmetries scale approximately in the ratio 1:1:2:3:3 for the A_1, A_2, E, F_1, F_2 symmetries, respectively.

LAPACK routine DSYEV and SCALAPACK routine PDSYEVD, as implemented in the Intel MKL library, were used to diagonalize the Hamitlonian matrices. The MPI version of LAPACK eigensolver PDSYEVD was used for large matrices with $J \geq 24$. All eigenroots were found in the direct diagonalizations but only eigenvectors below the energy threshold of $hc \cdot 18\,000$ cm^{-1} were stored and used in the line list production to reduce the calculations and storage. Fig. 3 gives the total number of energy levels and the number of transitions generated from these energy levels as a function of J, summed over all five symmetries. The linear dependence on J at lower values is capped at $J = 21{-}22$ by the energy threshold. At about $J = 50$, all energy levels of CH_4 are above 18 000 cm^{-1}. The total number of energy levels subject to the thresholds $E_{\rm max} = 18\,000$ cm^{-1} and $J_{\rm max} = 39$ is 6603 166.

4 LINE LIST CALCULATIONS

A spectroscopic line list is a catalogue of transitions containing transition frequencies (or wavenumbers $\tilde{\nu}_{\rm if}$) and transition line strengths (or Einstein A coefficients $A_{\rm if}$) between a well-chosen set of initial, i, and final, f, states. A line list also necessarily includes the total state degeneracy as well as the lower state energy to allow simulation of absorption or emission spectra at different temperatures. It is also common to include the quantum numbers specifying states involved in each transitions. For more details see Tennyson (2012) and Tennyson, Hill & Yurchenko (2013).

The goal of this work is a comprehensive line list for CH_4 covering the wavenumber range up to 12 000 cm^{-1} and applicable for temperatures up to $T = 1500$ K. To be complete at $T = 1500$ K, we estimated that the population is negligible for energies above 8000 cm^{-1}. This defines our maximal value for lower state energy. We find that at $J = 40$ all energy term values are above 8000 cm^{-1}. The lower state energy threshold of $hc \cdot 8000$ cm^{-1} combined with the wavenumber range 10 000 cm^{-1} defines the energy threshold for the upper state to be $hc \cdot 18\,000$ cm^{-1}, which is also the maximal energy of CH_4 included in the final line list. That is, the thresholds for the energy and eigenvectors are $J_{\rm max} = 39$, $E''_{\rm max} = hc \cdot 8000$ cm^{-1}, $E'_{\rm max} = hc \cdot 18\,000$ cm^{-1}. For the transition calculations, we choose an extended wavenumber range up to $\tilde{\nu}_{\rm max} = 12\,000$ cm^{-1}; however, the maximal temperature is applicable for the transitions up to 10 000 cm^{-1} (wavelengths longwards of 1 μm) only.

For the total number of levels considered, 6603 166, the total number of transitions computed is 9819 605 160, i.e. almost 10^{10}, which is why we call the line list '10to10'. Obviously, not all these transitions are important at all temperature. However, to demonstrate that a large number of transitions do matter at elevated temperatures, Fig. 4 shows the density of lines per an absorption intensity $I_{\rm if} = A \times 10^x$ unit for different temperatures covering the whole wavenumber range 0, ..., 12 000 cm^{-1}. The slightly deformed Gaussian-like distributions peak at $x = -39, -33, -32, -30$ and -29 for $T = 297$, 600, 1000 and 1500 K, respectively, with long, very small tails spreading up to $x = -18$ which are not visible at this scale. 98 per cent of the $T = 296$ K lines we compute have intensities smaller than 10^{-32} cm molecule^{-1} and barely contribute to the total opacity at room temperature, and thus can be safely ignored. Conversely at $T = 1500$ K, where the absorption lines peak at $I_{\rm if} 10^{-29}$ cm molecule^{-1}, most of the hot lines (98 per cent) appear to be stronger than 10^{-32} cm molecule^{-1}. Many of these lines also overlap each other, due to the very high density of states, which is not reflected on this figure. In order to bring the line list to a more manageable size, we could apply an intensity cut-off and compiled a reduced version of the line list which gives absorption intensities higher than a certain threshold, say 10^{-27} cm molecule^{-1}. It is known however that even weaker lines may play important role for non-LTE environments (Dello Russo et al. 2004), which is the reason for keeping even extremely weak absorption transitions in

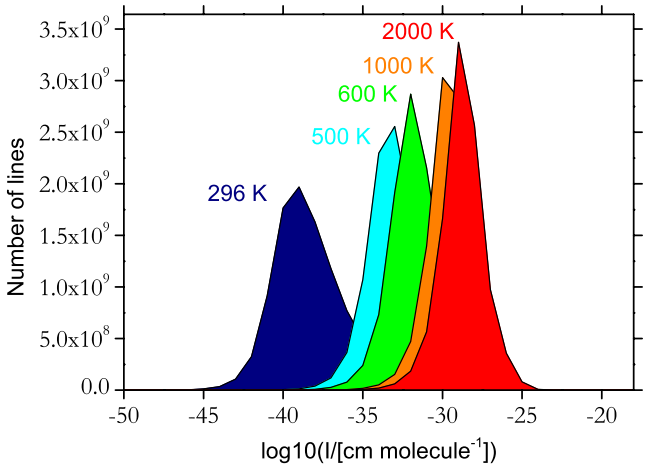

Figure 4. Number of intense lines as a function of intensity for different temperatures. The *x*-axis gives the log of the intensity in cm molecule^{-1}, while the *y*-axis represents the number of transitions per each 10^x cm molecule^{-1} bin.

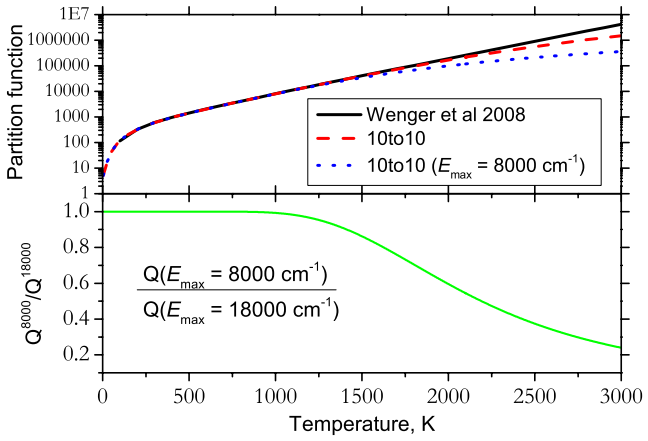

Figure 5. Temperature dependence of the partition function of CH_4.

10to10. In fact there are other, better ways of making this manageable such as cross-sections (Hill, Yurchenko & Tennyson 2013) or *k*-coefficients (Irwin et al. 1996).

Wenger, Champion & Boudon (2008a) calculated the partition function for methane for temperatures up to 3000 K by using all states up to the dissociation, whose energies where modelled using different levels of approximations. Fig. 5 (upper display) compares this partition function with our values obtained by (a) summing all energies from the 10to10 line list ($Q^{(18\,000)}$) and (b) summing all energies below our lower cut-off of 8000 cm^{-1} ($Q^{(8\,000)}$). This latter value is useful as it allows us to estimate the completeness of the 10to10 line list as a function of temperature. To quantify this effect, the lower display of Fig. 5 also shows the ratio of the two partition functions, $Q^{(8\,000)}$ and $Q^{(18\,000)}$. As discussed above, our set of energies are the subject of the threshold of $hc \cdot 18\,000$ cm^{-1}, which affects the accuracy of our partition function at higher temperature. At 1 000 K, 10to10 appears to be complete but by 1500 K the 8000 cm^{-1} threshold leads to up to 15 per cent undersampling which increases rapidly with temperature. Similar behaviour can be expected for the absorption intensities when modelled at 1500 K and higher temperatures.

5 THE FORMAT OF THE LINE LIST

We adopt the ExoMol format (Tennyson et al. 2013) for the 10to10 line list. In this format, the line list consists of two files: (i) an Energy file containing all information necessary to describe a given energy level including, most importantly, the lower state energies and the total degeneracies; (ii) a Transition file, where the Einstein coefficients for all transitions are specified. In the Energy file, each energy level is numbered from 1 to 6603 166, sorted by J (from 0 to 39), symmetry (A_1, A_2, E, F_1 and F_2) and energy. The counting number i, which is the same as the row number, is an unique tag characterizing a given level. The counting number is then followed by the lower state term value (cm^{-1}) and the total statistical weights g_i, which for CH_4 in its ground ($^1\Sigma$) electronic state disregarding the hyperfine splitting, is given by

$$g_i = (2J_i + 1)g_{\rm ns}^{(i)}. \quad (7)$$

Each energy record also includes the 'good quantum numbers' J and $\Gamma_{\rm tot}$ (the total symmetry), as well as other quantum numbers from equation (3). An extract from the Energy file is given in Table 3.

The Transition file lists the electric dipole transition probabilities in the form the Einstein A coefficient $A_{\rm if}$ in s^{-1} for each transition i $\rightarrow$ f complemented by the i and f tags identifying the states in the Energy file, for the lower (initial) and upper (final) states, respectively. For the convenience, the Transition file is split into 100 cm^{-1} wavenumber pieces (121 files). An extract from one of the Transition files is given in Table 4. According to the ExoMol naming convention, the Energy file is called 10to10.states, while the Transition files are called 10to10-*nnnn*.transitions, where *nnnn* indicates the wavenumber region presented.

The ExoMol website also provides alternative tools allowing the user to convert the line list into different representations, which currently include HITRAN format (Rothman et al. 2013) and the cross-sections, see Hill et al. (2013). We also provide a spectrum program to simulate absorption and emission spectra using the 10to10 line list, in the form of the 'stick' spectrum as well as of cross-sections (with different broadenings). The full line list can be also downloaded from the Strasbourg Data Centre (SDC), via ftp://cdsarc.u-strasbg.fr/pub/cats/J/MNRAS/, or http://cdsarc.u-strasbg.fr/viz-bin/qcat?J/MNRAS/.

6 ANALYSIS

In this section, we compare the $^{12}CH_4$ spectra generated using the 10to10 line list with data available from other sources.

6.1 HITRAN

The latest (2012) update of HITRAN contains 336 830 lines of $^{12}CH_4$ (Rothman et al. 2013). Fig. 6 compares a $T = 296$ K HITRAN spectrum for $^{12}CH_4$ with the spectrum generated from 10to10 at the same temperature. The 10to10 spectral lines are given as sticks with the intensity (cm molecule^{-1}) represented by their height. In order to simplify the plot of the 10to10 spectra, only the strongest lines within each 0.01 bin are shown. The HITRAN 2012 data are given as circles. Apart from general good agreement between theory and experiment, one can see that the coverage of the experimental CH_4 data as represented by HITRAN though reasonably good, still has gaps in both the frequency and intensity directions.

Fig. 7 gives a number of zoomed-in pictures of several bands, which illustrate the quality of our data. Both the line positions and

Table 3. Extract from the 10to10 Energy file. The full data set is available online.

1	2	3	4	5	6	7	8	9	10	11	12	13	14	15	16	17	18	19	20	21	22	23	24	25	26	27	28	29	30
N	$\tilde{E}$	$g_{\rm tot}$	J	$\Gamma_{\rm tot}$	n_1	n_2	L_2	n_3	L_3	M_3	n_4	L_4	M_4	$\Gamma_{\rm vib}$	J	K	$\tau_{\rm rot}$	$\Gamma_{\rm rot}$	$N_{J,\Gamma}$	$\lvert C_i\rvert^2$	v_1	v_2	v_3	v_4	v_5	v_6	v_7	v_8	v_9
8836	1311.457 042	15	1	2	0	0	0	0	0	0	1	1	1	5	1	1	1	4	1	1.00	0	0	0	0	0	0	1	0	0
8837	2632.988 747	15	1	2	0	0	0	0	0	0	2	2	1	5	1	1	1	4	2	1.00	0	0	0	0	0	0	0	1	1
8838	2847.722 094	15	1	2	0	1	1	0	0	0	1	1	1	5	1	1	1	4	3	1.00	0	0	0	0	1	0	1	0	0
8839	3028.725 668	15	1	2	0	0	0	1	1	1	0	0	0	5	1	1	1	4	4	1.00	0	1	0	0	0	0	0	0	0
8840	3871.607 969	15	1	2	0	0	0	0	0	0	3	1	1	5	1	1	1	4	5	1.00	0	0	0	0	0	0	3	0	0
8841	3955.888 843	15	1	2	0	0	0	0	0	0	3	3	1	5	1	1	1	4	6	1.00	0	0	0	0	0	0	1	2	0
8842	4148.535 610	15	1	2	0	1	1	0	0	0	2	2	1	5	1	1	1	4	7	1.00	0	0	0	0	1	0	0	1	1
8843	4223.887 822	15	1	2	1	0	0	0	0	0	1	1	1	5	1	1	1	4	8	1.00	0	0	1	0	0	0	1	0	0
8844	4333.813 607	15	1	2	0	0	0	1	1	1	1	1	1	5	1	1	1	4	9	1.00	0	1	0	0	0	0	1	0	0
8845	4353.438 372	15	1	2	0	2	0	0	0	0	1	1	1	5	1	1	1	4	10	0.97	0	0	0	0	2	0	1	0	0
8846	4389.406 791	15	1	2	0	2	2	0	0	0	1	1	1	5	1	1	1	4	11	0.97	0	0	0	0	0	2	1	0	0
8847	4555.544 940	15	1	2	0	1	1	1	1	1	0	0	0	5	1	1	1	4	12	1.00	0	1	0	0	1	0	0	0	0
8848	5158.823 917	15	1	2	0	0	0	0	0	0	4	2	1	5	1	1	1	4	13	1.00	0	0	0	0	0	0	0	1	3
8849	5199.314 103	15	1	2	0	0	0	0	0	0	4	4	1	5	1	1	1	4	14	1.00	0	0	0	0	0	0	2	1	1
8850	5387.416 906	15	1	2	0	1	1	0	0	0	3	1	1	5	1	1	1	4	15	0.99	0	0	0	0	1	0	3	0	0
8851	5419.899 376	15	1	2	0	1	1	0	0	0	3	3	3	5	1	1	1	4	16	0.98	0	0	0	0	1	0	0	2	1
8852	5467.412 035	15	1	2	0	1	1	0	0	0	3	3	1	5	1	1	1	4	17	0.98	0	0	0	0	1	0	1	2	0
8853	5541.185 628	15	1	2	1	0	0	0	0	0	2	2	1	5	1	1	1	4	18	1.00	0	0	1	0	0	0	0	1	1
8854	5596.854 392	15	1	2	0	0	0	1	1	1	2	0	0	5	1	1	1	4	19	0.99	0	1	0	0	0	0	0	2	0
8855	5617.895 727	15	1	2	0	0	0	1	1	1	2	2	2	5	1	1	1	4	20	0.95	0	1	0	0	0	0	0	0	2
8856	5650.480 713	15	1	2	0	2	0	0	0	0	2	2	1	5	1	1	1	4	21	0.86	0	0	0	0	2	0	0	1	1
8857	5659.593 538	15	1	2	0	0	0	1	1	1	2	2	1	5	1	1	1	4	22	0.85	0	1	0	0	0	0	0	1	1
8858	5683.390 696	15	1	2	0	2	0	0	0	0	2	2	1	5	1	1	1	4	23	0.96	0	0	0	0	2	0	0	1	1
8859	5747.346 056	15	1	2	1	1	1	0	0	0	1	1	1	5	1	1	1	4	24	1.00	0	0	1	0	1	0	1	0	0
8860	5829.908 396	15	1	2	0	1	1	1	1	1	1	1	1	5	1	1	1	4	25	1.00	0	1	0	0	1	0	1	0	0
8861	5852.531 380	15	1	2	1	0	0	1	1	1	0	0	0	5	1	1	1	4	26	0.95	0	0	2	0	0	0	0	0	0
8862	5862.518 649	15	1	2	0	1	1	1	1	1	1	1	1	5	1	1	1	4	27	0.95	0	1	0	0	1	0	1	0	0
8863	5876.015 235	15	1	2	0	3	1	0	0	0	1	1	1	5	1	1	1	4	28	0.92	0	0	0	0	3	0	1	0	0
8864	5901.578 781	15	1	2	0	3	3	0	0	0	1	1	1	5	1	1	1	4	29	0.92	0	0	0	0	1	2	1	0	0
8865	6015.774 283	15	1	2	0	0	0	2	2	1	0	0	0	5	1	1	1	4	30	1.00	1	1	0	0	0	0	0	0	0
8866	6064.380 191	15	1	2	0	2	0	1	1	1	0	0	0	5	1	1	1	4	31	1.00	0	1	0	0	2	0	0	0	0

Column	Notation	
1	N	Level number (row).
2	$\tilde{E}$	Term value (in $\rm cm^{-1}$).
3	$g_{\rm tot}$	Total degeneracy.
4	J	Rotational quantum number.
5	$\Gamma_{\rm tot}$	Total symmetry in $\mathcal{T}_{\rm d}(M)$.
6,7,9,12	n_1–n_4)	Normal mode vibrational quantum numbers (see Appendix A).
8,10,13	L_2, L_3, L_4	Vibrational angular momenta quantum numbers.
11,14	M_3, M_4	Multiplicity index quantum numbers.
15	$\Gamma_{\rm vib}$	Symmetry of the vibrational contribution in $\mathcal{T}_{\rm d}(M)$.
16	J	Rotational quantum number (the same as column 2).
17	K	Rotational quantum number, projection of J on to the z-axis.
18	$\tau_{\rm rot}$	Rotational parity (0,1).
19	$\Gamma_{\rm rot}$	Symmetry of the rotational contribution in $\mathcal{T}_{\rm d}(M)$.
20	$N_{J,\Gamma}$	Running number in the J, Γ block.
21	$\lvert C_i\rvert^2$	Largest coefficient used in the assignment.
22–30	v_1–v_9	Local mode vibrational quantum numbers (see Yurchenko et al. 2013).

Table 4. Extract from the 10to10 Transition file. The full data set is available online.

F	I	A_{IF} (s^{-1})
1002 348	1180 308	1.2167e−04
1033 584	1024 255	4.5595e−04
10 461	27 572	1.2159e−03
1046 761	1199 185	1.5956e−03
1049 153	863 924	4.4509e−04
1049 953	1024 823	4.1242e−04
1050 761	1024 875	7.6355e−05
105 546	135 097	1.0140e−03
1088 309	1292 264	2.6590e−06
1099 011	1111 107	7.0156e−06
1116 545	1058 555	4.6582e−04
1150 480	1236 818	1.5768e−04

I: Upper state counting number; F: Lower state counting number; A_{IF}: Einstein A coefficient in s^{-1}.

the absolute intensities agree well with the HITRAN data, at least for the strongest lines. A more detailed line-by-line comparative analysis is planned in the near future. Our spectrum seems to disagree with HITRAN 2012 in the wavenumber region 800–900 cm^{-1}, where new release of HITRAN has a stronger feature which was not present in the previous, 2008 release of HITRAN (Rothman et al. 2009) or in our calculations. This feature corresponds to two hot, combination bands $3\nu_4 - 2\nu_2$ and $3\nu_4 - \nu_3$. These bands are yet to be characterized experimentally and thus result purely from an extrapolation. We suggest that there is a problem with the effective dipole moment model used to generate these lines. Furthermore, we note that the new HITRAN 2012 lines in the region 300–600 cm^{-1} have significantly different (lower) intensities compared to the data in HITRAN 2008 where the latter also agrees well with the 10to10 spectrum.

The intensities of our stick spectrum in the band around the 7000 cm^{-1} band appear to be very different from those of HITRAN. The bottom-right display of Fig. 7 also shows the spectrum convolved with a $T = 296$ K Doppler profile, which allows overlapping lines to be added together. This spectrum is in much better agreement with the HITRAN stick intensities, suggesting that most of the intensities given as single lines in HITRAN are actually

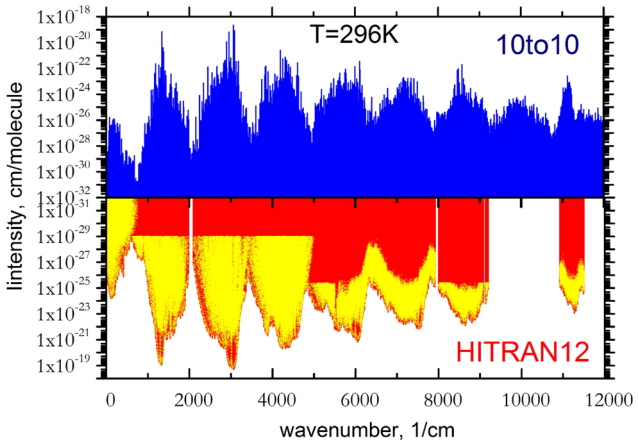

Figure 6. Absorption of $^{12}CH_4$ at $T = 296$ K: HITRAN 2012 (bottom) Rothman et al. (2013) and 10to10 (top). The yellow stars are to indicate the intensity coverage in HITRAN.

from blends. Our stick spectrum starts 'de-focusing' at 8000 cm^{-1} in terms of the centre of the bands, this probably indicates the limitations of our refined PES in this region.

6.2 Hot spectrum of CH_4

6.2.1 Experimental comparisons

It is common for the absorption spectra of polyatomic molecules to change dramatically with increased temperature. Fig. 8 illustrates the dynamic temperature effect in the case of the methane absorption spectrum. Especially, the window regions between strong bands gain significant intensity as temperature increases. These windows regions are generally undersampled in laboratory experiments because of their very weak absorption. The corresponding lines compiled mostly from the hot-bands transitions become increasingly important at elevated temperatures when the hot-bands get stronger. The HITRAN-based spectrum significantly underestimates the opacity of CH_4 in the regions between the strong bands and, as a result, gives the bands the wrong shape. This is especially evident at the higher wavenumbers bands, 5000–6000 cm^{-1} and 7000–8000 cm^{-1}, where the HITRAN representation of methane is especially sparse. To illustrate the problem of the undersampling, Table 6 lists opacities (integrated intensities) for the H, J and K spectral regions (see also below). We used a simple definition of the K (2.0–2.4 μm), H (1.5–1.8 μm) and J (1.1–1.4 μm) regions given also in Table 6.

Experimentally, the spectrum of hot methane has been the subject of several studies, see Nassar & Bernath (2003) ($T = 800$, 1 000 and 1273 K), Thiévin et al. (2008) ($T = 1005$–1820 K) and Hargreaves et al. (2012) ($T = 573$–1673 K) cm^{-1}. Table 5 summarizes the coverage of these studies. The 10to10 results given in this table suggest that the absorption by methane in each band is essentially independent of temperature; all previous studies show significantly less absorption by methane at elevated temperatures.

Fig. 9 shows the $T = 1425$ K absorption spectrum of Thiévin et al. (2008) compared to two types of synthetic (10to10) absorption spectra of CH_4 at $T = 1500$ K: (a) a 'stick' spectrum and (b) a Doppler-broadened spectrum. The good agreement with the latter spectrum shows the importance of the correct description of the line mixing for accurate reconstruction of the line absorption, absent in the experimental line list by Thiévin et al. (2008).

Fig. 10 compares the 10to10 absorption (stick) spectrum of CH_4 at $T = 1000$ K with the 1000 K absorption spectrum of Nassar & Bernath (2003) and to the $T = 973$ K spectrum of Hargreaves et al. (2012). We see that there is generally good agreement between theory and experiment. However, the integrated absorption intensities are very different, see Table 6. In the region 4166.7–5000.0 cm^{-1} (K band), at $T = 1273$ K the line list of Hargreaves et al. (2012) gives $I_{tot} = 3.7\times 10^{-19}$ cm molecule^{-1}, compared to our value, 8.2×10^{-19} cm molecule^{-1}. HITRAN 2012 underestimates the opacity at these temperature and region even more, giving $I_{tot} = 1.7\times 10^{-19}$ cm molecule^{-1}. For the higher wavenumber regions (H and J), the problem of missing opacities is even more pronounced from one (Nassar & Bernath 2003) to two (HITRAN 2012) orders of magnitude.

A final piece of experimental information are the 'PNNL' cross-sections provided by Sharpe et al. (2004) (cm^2 molecule^{-1}) which are presented at three temperatures, $T = 5$, 20 and 50 C. Fig. 11 compares the $T = 50$ C PNNL cross-sections with that generated by 10to10.

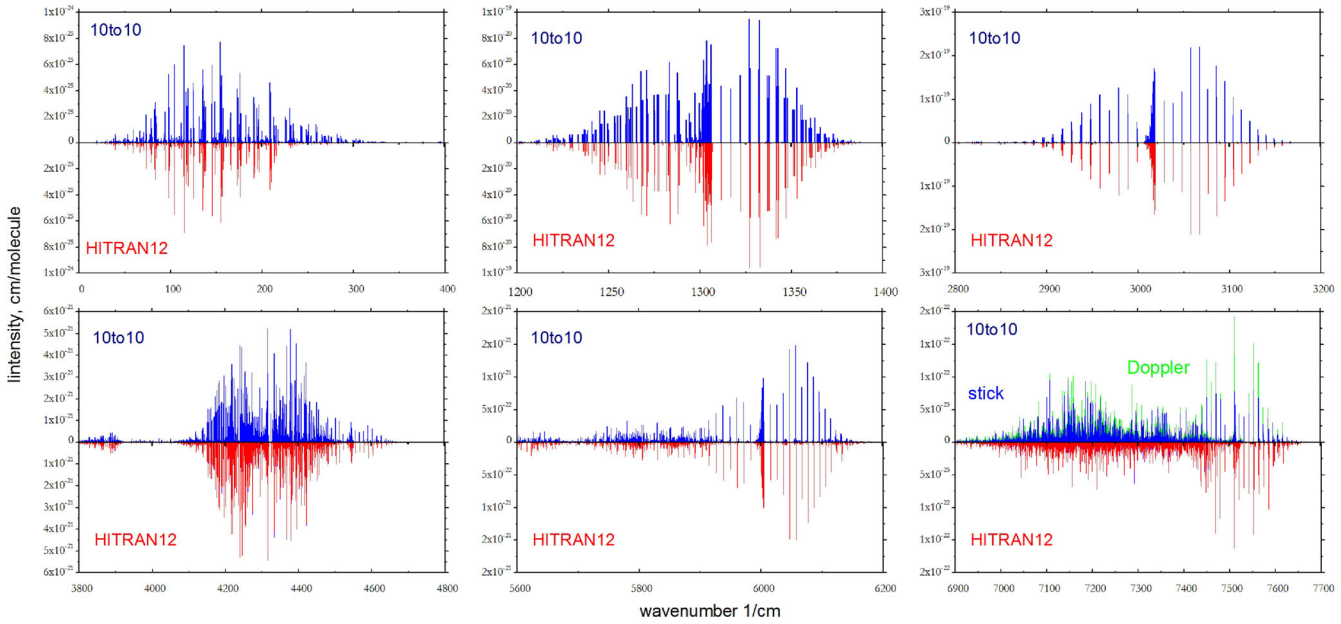

Figure 7. The absorption spectrum of $^{12}CH_4$ at $T = 296$ K: 10to10 (blue) versus HITRAN 2012 (red) compared for different wavenumber windows. The bottom-right display also shows the 296 K spectrum convolved with the doppler profile (green).

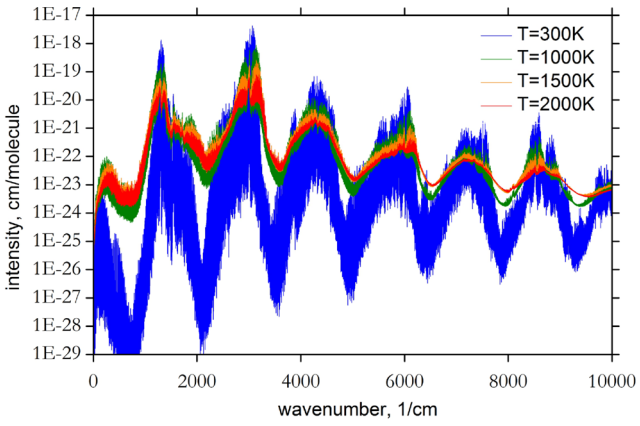

Figure 8. Temperature dependence of the absorption cross-sections (cm molecule^{-1}) of $^{12}CH_4$ computed at $T = 300$, 1000, 1500 and 2000 K using the 10to10 line list.

6.2.2 *Theoretical comparisons*

Warmbier et al. (2009) reported a theoretical hot-line list for methane computed variationally using the program MULTIMODE (Carter & Bowman 1998) in conjunction with an ab initio PES and DMS calculated at the RCCSD(T)/aug-cc-pVTZ level of theory. This line list contains 1.4 million lines covering the wavenumbers up to 6200 cm^{-1} with $J = 0, \ldots, 34$ and energies up to 6200 cm^{-1} only. We used this line list to generate the cross-sections of CH_4 at $T = 1500$ K assuming Doppler broadening only. Fig. 12 compares these cross-sections with those from 10to10 at the same temperature. The significantly lower values of the cross-sections by Warmbier et al. (2009) indicate that their line list is very incomplete especially for higher frequencies and for hot bands. The corresponding integrated intensities for the H and K bands listed in Table 6 give a quantitative illustration of this conclusion. For example, the H-band integrated intensity at $T = 1500$ K obtained from the line list of Warmbier et al. (2009) is 6.3×10^{-21} cm molecule^{-1} which is 10 times weaker than the 10to10 value.

Very recently an accurate synthetic line list MeCaSDa was reported by Ba et al. (2013). It was generated using the XTDS software (Wenger et al. 2008b). This line list contains 5045 392 transitions of $^{12}CH_4$ with $J \leq 25$ and covering the wavenumber range up to 6446 cm^{-1} with lower state energies up to 6340 cm^{-1}, see Table 5. The line positions are close to experimental accuracy with a reasonable coverage of CH_4 hot transitions. Fig. 12 compares the $T = 1000$ K spectrum generated using MeCaSDa (below

Table 5. Summary of available experimental and theoretical methane line lists.

Line list	T (K)	Wavenumber (cm^{-1})	N lines	J_{max}	E_{max}
Nassar & Bernath (2003)	800, 1000, 1273	2 000–6400	16 191,23 002,26 821		
Hargreaves et al. (2012)	573, 673, . . . , 1673	960–5000	33 955–79 098		
Thiévin et al. (2008)	1005, 1365, 1485, 1625	2 700–3300	4904, 3824, 5647, 2381, 1559		
HITRAN 2012		0–11 502	336 830	25	4263
Warmbier et al. (2009)		0–6133	1410 789	34	6200
MeCaSDa		0–6446	5045 392	25	6340
10to10		0–12 000	9819 605 160	39	8000

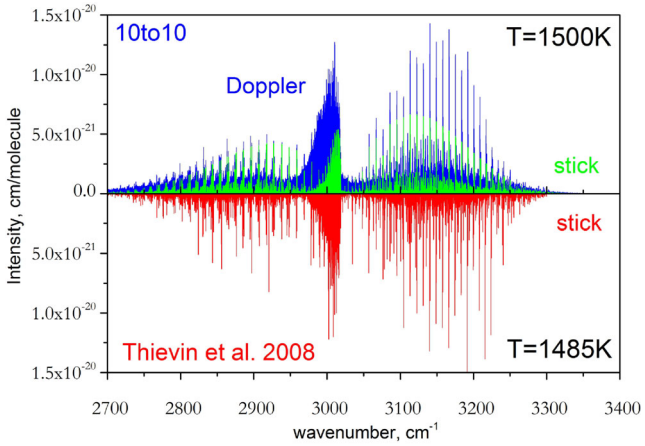

Figure 9. The absorption spectrum of $^{12}CH_4$ at $T = 1485$ K. The bottom display shows the experimental intensities (cm molecule^{-1}) derived by Thiévin et al. (2008) from their emission spectra in the region 2700–3300 cm^{-1}. The top display shows: (sticks) the 10to10 absorption spectrum lines obtained as the maximal intensity at the 0.2 cm^{-1} wavenumber bin and (Doppler) the 10to10 absorption spectrum convolved with the Doppler profile and integrated over a 0.1 cm^{-1} wavenumber bin.

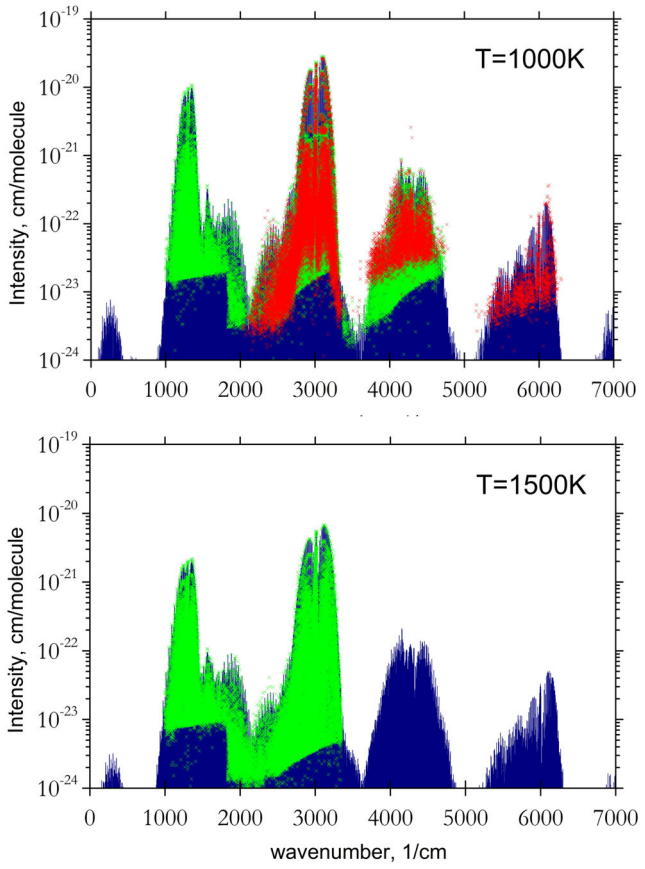

Figure 10. Experimental (crosses) and theoretical (blue bars) absorption intensities of $^{12}CH_4$ at $T = 1000$ and 1500 K. The experimental data are from Nassar & Bernath (2003, red) and Hargreaves et al. (2012, green). Note that the actual temperatures used by Hargreaves et al. (2012) were $T = 973$ and 1473 K.

6446 cm^{-1}) and that obtained with 10to10. The differences are less pronounced than for HITRAN or Warmbier et al. (2009); however, some opacity at high temperature is still missing, see Table 6. For example, for the *H*-band integrated intensity at $T = 1000$ K MeCaSDa gives $I_{tot} = 2.5 \times 10^{-20}$ cm molecule^{-1}, which is six times smaller than that of 10to10. At $T = 1500$ K, this difference is even more dramatic, 1.3×10^{-20} (MeCaSDa) compared to 1.5×10^{-19} cm molecule^{-1} (10to10).

6.2.3 *Astrophysical comparisons*

Methane has been detected in the atmospheres of exoplanets, cool stars and comets. We have selected two extraterrestrial methane spectra recorded at elevated temperatures at relatively high or medium resolution. The several collisions of comet Shoemaker–Levy 9 with Jupiter was carefully observed in the IR (Orton et al. 1995). Fig. 13 compares a synthetic 10to10 emission spectrum of methane at $T = 1400$ K with one of the Jovian spectra recorded during the impact of comet Shoemaker–Levy 9 on 1994 July 17 (Dinelli et al. 1997). Dinelli et al. (1997) identified a number of hot methane features based on the high-resolution spectrum of Hilico et al. (1994).

Our other example is associated with the spectroscopy of the methane brown dwarfs. Fig. 14 gives a comparison of a synthetic 10to10 absorption spectrum of CH_4 at $T = 1200$ K with the spectrum of the T4.5 brown dwarf 2MASS J0559−1404 centred at 1.67 μm reported by Cushing, Rayner & Vacca (2005), who characterized the methane spectral features based on the high-resolution CH_4 spectrum by Nassar & Bernath (2003). In both cases, our spectra agree well with the observation and can potentially offer a more complete picture of the methane contributions to the spectral description of cool stars and exoplanets.

7 CONCLUSION

We have computed a methane vibration–rotation line list containing almost 10 billion transitions which we call 10to10. The full line list for each of these isotopologues can be downloaded from the CDS, via ftp://cdsarc.u-strasbg.fr/pub/cats/J/MNRAS/ or http://cdsarc.u-strasbg.fr/viz-bin/qcat?J/MNRAS/ and from the ExoMol website www.exomol.com. The problem with having such an extensive line list is that files are large and difficult to manipulate. The ExoMol project provides facilities for generating cross-sections at appropriate temperatures (Hill et al. 2013).

10to10 has been constructed as the next member in the series of line lists provided by the ExoMol project (Tennyson & Yurchenko 2012; Yadin et al. 2012; Barton, Yurchenko & Tennyson 2013; Barber et al. 2014), which aims to provide comprehensive line lists for studies of hot atmospheres such as exoplanet, brown dwarfs and cool stars. Its construction means that there are now hot line lists for the key set of molecules methane, water (Barber et al. 2006) and ammonia (Yurchenko, Barber & Tennyson 2011b). These provide a suitable set of spectroscopic data on hot molecules for systematic models to be performed on astronomical objects with hot, molecular hydrogen-rich atmospheres. Work in this direction has already started (Yurchenko et al. 2014).

However, despite the size of the 10to10 line list it remains incomplete and should only be used with caution for temperatures higher than 1500 K as it will miss a significant proportion of the opacity at these higher temperatures. Furthermore, the effective, empirical character of the underlying PES and the convergence deficiency of the TROVE nuclear motion calculations means that the accuracy of the

Table 6. Integrated intensities for the *K*, *H* and *J* bands from different line lists.

	296 K	1000 K	1200 K	1273 K	1500 K	2000 K
Line list			*K* band: 4166.7–5000.0 cm^{-1}			
Nassar & Bernath (2003)		2.6e−19		1.6e−19		
Hargreaves et al. (2012)[a]		5.2e−19		3.7e−19		
Thiévin et al. (2008)						
HITRAN 2012	8.1e−19	1.6e−19	2.0e−19	1.7e−19	9.7e−20	3.0e−20
Warmbier et al. (2009)	8.1e−19	3.5e−19	4.6e−19	3.8e−19	2.3e−19	7.1e−20
MeCaSDa	8.1e−19	2.8e−19	4.0e−19	3.4e−19	2.2e−19	7.6e−20
10to10	7.8e−19	8.0e−19	8.2e−19	8.2e−19	7.8e−19	5.7e−19
			H band: 5555.6–6666.7 cm^{-1}			
Nassar & Bernath (2003)				2.3e−20		
Hargreaves et al. (2012)						
Thiévin et al. (2008)						
HITRAN 2012	1.0e−19	1.0e−20	1.1e−20	8.9e−21	4.7e−21	1.2e−21
Warmbier et al. (2009)	2.3e−19	1.5e−20	1.6e−20	1.2e−20	6.3e−21	1.6e−21
MeCaSDa	1.3e−19	2.5e−20	3.0e−20	2.4e−20	1.3e−20	3.8e−21
10to10	1.4e−19	1.5e−19	1.6e−19	1.6e−19	1.5e−19	1.1e−19
			J band: 7142.9–9090.9 cm^{-1}			
Nassar & Bernath (2003)						
Hargreaves et al. (2012)						
Thiévin et al. (2008)						
HITRAN 2012	1.4e−21	7.3e−23			3.0e−23	7.3e−24
Warmbier et al. (2009)						
MeCaSDa						
10to10	6.0e−20	6.3e−20			6.6e−20	5.2e−20

[a]The actual temperature used by Hargreaves et al. (2012) was $T = 973$ K.

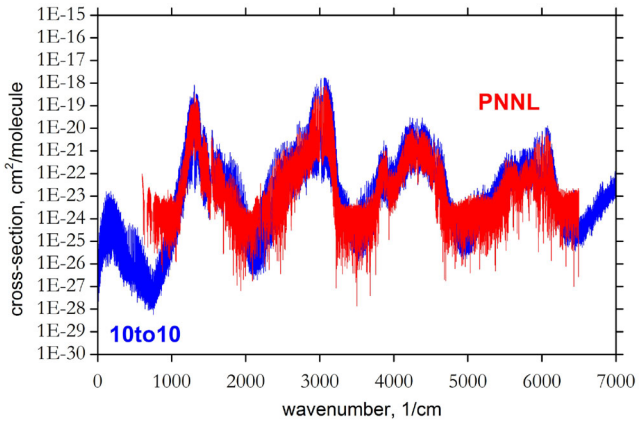

Figure 11. Comparison of the 10to10 and Sharpe et al. (2004) cross-sections of $^{12}CH_4$ at $T = 50$ C.

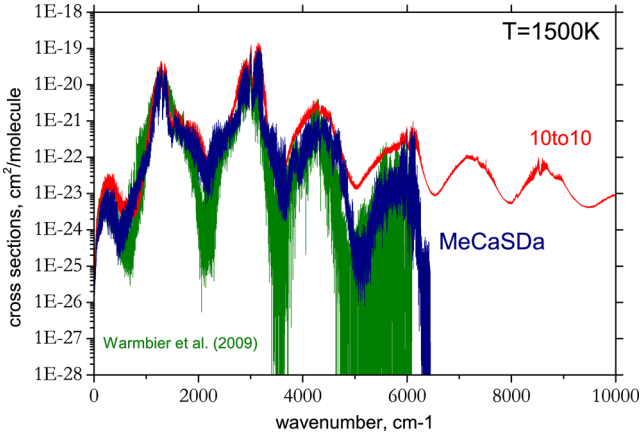

Figure 12. Theoretical cross-sections σ (cm^2 molecule^{-1}) of $^{12}CH_4$ at $T = 1500$ K obtained using three line lists: (i) 10to10, (ii) MeCaSDa (Ba et al. 2013) and (iii) Warmbier et al. (2009).

energy levels, particularly at higher energies, and hence, the related transition frequencies could be improved. Work in this direction will be undertaken in due course.

ACKNOWLEDGEMENTS

This work was supported by STFC and ERC Advanced Investigator Project 267219. The research made use of the DiRAC@Darwin and DiRAC@COSMOS HPC clusters. DiRAC is the UK HPC facility for particle physics, astrophysics and cosmology and is supported by STFC and BIS. We also thank UCL for use of the Legion High Performance Computer for performing the electronic structure calculations and Bianca Maria Dinelli for providing her cometary data.

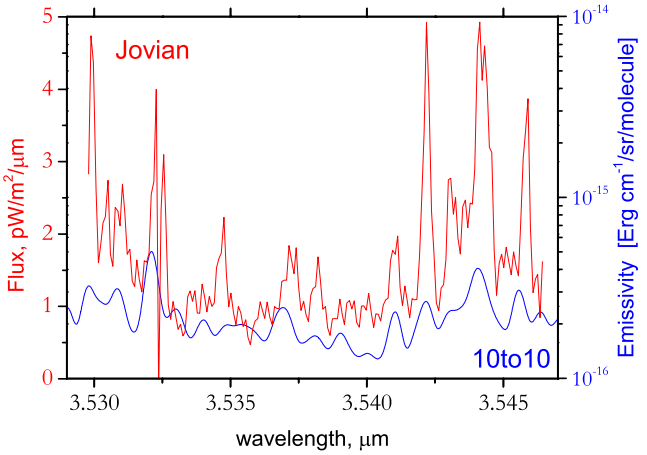

Figure 13. Jupiter spectrum recorded 1994 July 17 during the impact of comet Shoemaker–Levy 9 (Dinelli et al. 1997) (red) and 10to10 emission spectrum of CH_4 at $T = 1400$ K.

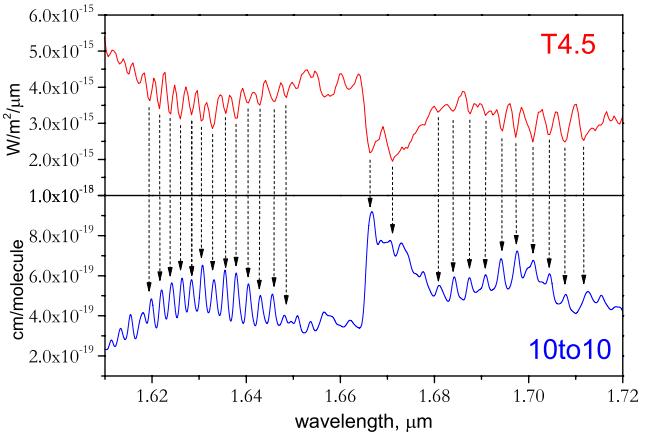

Figure 14. The spectrum of the T5 Brown Dwarf 2MASS J0559−1404 (Cushing et al. 2005) compared to the 10to10 absorption spectrum of CH_4 at $T = 1200$ K. All features are from CH_4. Arrows are shown to guide the eye.

REFERENCES

Atreya S. K., Mahaffy P. R., Wong A.-S., 2007, Planet Space Sci., 55, 358
Ba Y. A. et al., 2013, J. Quant. Spectrosc. Radiat. Transf., 130, 62
Bailey J., Kedziora-Chudczer L., 2012, MNRAS, 419, 1913
Barber R. J., Tennyson J., Harris G. J., Tolchenov R. N., 2006, MNRAS, 368, 1087
Barber R. J., Strange J. K., Hill C., Polyansky O. L., Mellau G. C., Yurchenko S. N., Tennyson J., 2014, MNRAS, 437, 1828
Barton E. J., Yurchenko S. N., Tennyson J., 2013, MNRAS, 434, 1469
Beaulieu J. P. et al., 2011, ApJ, 731, 16
Bernath P. F., 2009, Int. Rev. Phys. Chem., 28, 681
Boudon V., Rey M., Loëte M., 2006, J. Quant. Spectrosc. Radiat. Transf., 98, 394
Brown L. R. et al., 2013, J. Quant. Spectrosc. Radiat. Transf., 130, 201
Bunker P. R., Jensen P., 2004, Fundamentals of Molecular Symmetry. IOP Publishing, Bristol
Campargue A., Leshchishina O., Mondelain D., Kassi S., Coustenis A., 2013, J. Quant. Spectrosc. Radiat. Transf., 118, 49
Carter S., Bowman J. M., 1998, J. Chem. Phys., 108, 4397
Cushing M. C., Rayner J. T., Vacca W. D., 2005, ApJ, 623, 1115
Dello Russo N., DiSanti M. A., Magee-Sauer K., Gibb E. L., Mumma M. J., Barber R. J., Tennyson J., 2004, Icarus, 168, 186
Dinelli B. M. et al., 1997, Icarus, 126, 107
Down M. J., Hill C., Yurchenko S. N., Tennyson J., Brown L. R., Kleiner I., 2013, J. Quant. Spectrosc. Radiat. Transf., 130, 260
Geballe T. R., Kulkarni S. R., Woodward C. E., Sloan G. C., 1996, ApJ, 467, L101
Hargreaves R. J., Beale C. A., Michaux L., Irfan M., Bernath P. F., 2012, ApJ, 757, 46
Hilico J. C., Champion J.-P., Toumi S., Tyuterev V. G., Tashkun S. A., 1994, J. Mol. Spectrosc., 168, 455
Hill C., Yurchenko S. N., Tennyson J., 2013, Icarus, 226, 1673
Hougen J., 2001, Methane Symmetry Operations. NIST, Gaithersburg, MD., version 1.0. Available at: http://physics.nist.gov/Methane
Irwin P. G. J., Calcutt S. B., Taylor F. W., Weir A. L., 1996, J. Geophys. Res., 101, 26137
Jourdanneau E., Gabard T., Chaussard F., Saint-Loup R., Berger H., Bertseva E., Grisch F., 2007, J. Mol. Spectrosc., 246, 167
Krasnopolsky V. A., 2012, Icarus, 217, 144
Lucas P. W. et al., 2010, MNRAS, 408, L56
Maillard J.-P. et al., 1995, Geophys. Res. Lett., 22, 1573
Matyus E., Fabri C., Szidarovszky T., Czako G., Allen W. D., Csaszar A. G., 2010, J. Chem. Phys., 133
Mielke S. L., Chakraborty A., Truhlar D. G., 2013, J. Phys. Chem. A, 117, 7327
Nassar R., Bernath P., 2003, J. Quant. Spectrosc. Radiat. Transf., 82, 279
Nikitin A. V., Rey M., Tyuterev V. G., 2011, Chem. Phys. Lett., 501, 179
Nikitin A. V., Rey M., Tyuterev V. G., 2013, Chem. Phys. Lett., 565, 5
Orton G. et al., 1995, Science, 267, 1277
Oyanagi C., Yagi K., Taketsugu T., Hirao K., 2006, J. Chem. Phys., 124, 064311
Rey M., Nikitin A. V., Tyuterev V. G., 2013a, Phys. Chem. Chem. Phys., 15, 10049
Rey M., Nikitin A. V., Tyuterev V. G., 2013b, J. Mol. Spectrosc., 291, 8597
Rhoderick G. C., Dorko W. D., 2004, Environ. Sci. Technol., 38, 2685
Rothman L. S. et al., 2009, J. Quant. Spectrosc. Radiat. Transf., 110, 533
Rothman L. S. et al., 2010, J. Quant. Spectrosc. Radiat. Transf., 111, 2139
Rothman L. S. et al., 2013, J. Quant. Spectrosc. Radiat. Transf., 130, 4
Sagan C., Thompson W. R., Carlson R., Gurnett D., Hord C., 1993, Nature, 365, 715
Schwenke D. W., 2002, Spectra Chim. Acta A, 58, 849
Schwenke D. W., Partridge H., 2001, Spectra Chim. Acta A, 57, 887
Sharpe S. W., Johnson T. J., Sams R. L., Chu P. M., Rhoderick G. C., Johnson P. A., 2004, Appl. Spectrosc., 58, 1452
Stevenson K. B. et al., 2010, Nature, 464, 1161
Swain M. R., Vasisht G., Tinetti G., 2008, Nature, 452, 329
Swain M. R. et al., 2010, Nature, 463, 637
Tennyson J., 2012, WIREs Comput. Mol. Sci., 2, 698
Tennyson J., Yurchenko S. N., 2012, MNRAS, 425, 21
Tennyson J., Hill C., Yurchenko S. N., 2013, in Gillaspy J. D., Wiese W. L., Podpaly Y. A., eds, AIP Conf. Proc. Vol. 1545, 8th Int. Conf. on Atomic and Molecular Data and Their Applications ICAMDATA-2012. Am. Inst. Phys., New York, p. 186
Thiévin J., Georges R., Carles S., Benidar A., Rowe B., Champion J.-P., 2008, J. Quant. Spectrosc. Radiat. Transf., 109, 2027
Wang X.-G., Carrington T., Jr, 2013, J. Chem. Phys., 138, 104106
Warmbier R., Schneider R., Sharma A. R., Braams B. J., Bowman J. M., Hauschildt P. H., 2009, A&A, 495, 655
Wenger C., Champion J. P., Boudon V., 2008a, J. Quant. Spectrosc. Radiat. Transf., 109, 2697
Wenger C., Boudon V., Rotger M., Sanzharov M., Champion J. P., 2008b, J. Mol. Spectrosc., 251, 102
Wolff M., Rhein S., Bruhns H., Naehle L., Fischer M., Koeth J., 2013, Sensors Actuators B, 187, 574
Yadin B., Vaness T., Conti P., Hill C., Yurchenko S. N., Tennyson J., 2012, MNRAS, 425, 34
Yurchenko S. N., Carvajal M., Jensen P., Herregodts F., Huet T. R., 2003, Chem. Phys., 290, 59
Yurchenko S. N., Thiel W., Jensen P., 2007, J. Mol. Spectrosc., 245, 126

Yurchenko S. N., Barber R. J., Yachmenev A., Thiel W., Jensen P., Tennyson J., 2009, J. Phys. Chem. A, 113, 11845
Yurchenko S. N., Barber R. J., Tennyson J., Thiel W., Jensen P., 2011a, J. Mol. Spectrosc., 268, 123
Yurchenko S. N., Barber R. J., Tennyson J., 2011b, MNRAS, 413, 1828
Yurchenko S. N., Tennyson J., Barber R. J., Thiel W., 2013, J. Mol. Spectrosc., 291, 69
Yurchenko S. N., Tennyson J., Bailey J., Hollis M. D. J., Hollis T. G., 2014, submitted

APPENDIX A: METHANE QUANTUM NUMBERS

Methane is a symmetric five atomic molecule characterized by nine vibrational degrees of freedom with a vanishing permanent dipole moment. It is a very high symmetry molecule of the $\mathcal{T}_{\rm d}(M)$ symmetry group. In this work, we use the Molecular Symmetry group (Bunker & Jensen 2004) to describe the irreducible representations (irreps) of CH_4. Thus, the ro-vibrational states of CH_4 will be assigned with the five irreps, A_1, A_2, E, F_1 and F_2, where A_1 and A_2 are one-dimensional (1D), E is a 2D, and F_1 and F_2 are 3D irreps. Because of the $i = \frac{1}{2}$ nuclear spins of the hydrogens, the total spin-rotation–vibration states of $^{12}CH_4$ is fermionic and degenerate if hyperfine splittings are neglected. This degeneracy gives rise to nuclear statistical weight factors of 5, 5, 2, 3 and 3 for $\Gamma = A_1, A_2, E, F_1$ and F_2, respectively. The symmetry Γ is a 'good quantum number' (Bunker & Jensen 2004) as well as the rotational angular momentum quantum number J, which are two main labels used to classify the ro-vibrational states of CH_4. The electric dipole selection rules are given in equations (1) and (2). The dipole moment components of the molecule in the body-fixed frame span the three components of the F_2 irrep, F_{2_x}, F_{2_y} and F_{2_y} and the potential energy function is fully symmetric (A_1).

Apart from these well-defined, good quantum numbers, like J and symmetry, it is a common practise in spectroscopy to assign the ro-vibrational states of a molecule using a full set of rotational and vibrational labels which aid characterizing the state in question. These quantum numbers are usually associated with some selected referenced ro-vibrational functions and are used to describe the similarity of the given ro-vibrational eigenfunction to these reference functions. In variational approaches, where the eigenfunction is given as an linear expansion in terms of the basis functions, the similarity can be assessed by identifying the largest contribution to such an expansion (see, for example Yurchenko et al. 2007). In this case, the basis functions play the role of the reference functions and the labels characterizing the corresponding basis functions are used as the approximate quantum numbers for the eigenstate. The standard problem with this, and other approaches, is the strong mixing of basis set functions at high excitations which gives rise to the ambiguity in assignment. Alternatively, the similarity can be established by computing overlaps between the target and reference wavefunctions, see, for example Matyus et al. (2010), where the reference functions can be any functions and are not limited by the choice of the basis set. The conventional choice of the reference functions includes the rigid-rotor functions for the rotation and the normal mode (degenerate) harmonic oscillator eigenfunctions. Even the latter approach suffers from the state mixing problem and thus cannot guarantee unambiguous definition of the quantum numbers.

The difficulty of assigning the methane energy levels is well recognized. Boudon et al. (2006) suggested the following quantum numbers for the vibrational assignment: n_i, l_i, m_i and C_i, $i = 3, 4$, where n_i is the vibrational quantum number, l_i is the vibrational angular momentum ($l_i = n_i, n_i - 2, n_i - 4, \ldots, 0$ or 1 for $i = 2{-}4$), C_i is a $\mathcal{T}_{\rm d}$ irrep and m_i is multiplicity index for a given set (n_i, l_i, C_i). We partly follow this scheme.

We use the largest contribution approach to assign the eigenfunction of methane. Our selection of the quantum numbers for CH_4 is given in equation (3). For the rotation basis, symmetrized rigid-rotor functions $|J, K, \Gamma_{\rm rot}\rangle$ are used, where $K = |k|$, k is the projection of $\boldsymbol{J}$ on the body-fixed z-axis, and $\Gamma_{\rm rot}$ is the rotational symmetry. For the vibrations, we use nine 1D local (non-normal) mode basis functions $\phi_{v_i}(\xi_i)$ ($i = 1, \ldots, 9$) (see the text), which give rise to nine local mode vibrational quantum numbers v_i.

In order to provide the conventional normal mode quantum numbers, our local mode (vibrational) quantum numbers are mapped to their normal mode counterparts by comparing the corresponding symmetry and polyad of basis functions with that of the reference (degenerate) harmonic oscillator functions.

The normal mode quantum numbers are $n_1, n_2, L_2, n_3, L_3, M_3, n_4, L_4, M_4$. The classification of the normal modes under $\mathcal{T}_{\rm d}$ symmetry is given in Table 1. The quantum numbers n_2 associated with an isotropic 2D harmonic oscillator $|n_2, l_2\rangle$ (E symmetry) is complemented with the projection of the vibrational angular momentum $l_2 = -n_2, -n_2 + 2, \ldots, n_2 - 2, n_2$ (Bunker & Jensen 2004). Since the definition of the sign of l_2 is ambiguous (as ambiguous as the sign of k), we follow the suggestion of Down et al. (2013) and use the absolute value $L_2 = |l_2| = n_2, n_2 - 2, \ldots, 0$ (1) instead. Similarly, the classification of the 3D normal modes 3 and 4 is based on the 3D isotropic harmonic oscillator $|n_i, l_i\rangle$ (Hougen 2001) ($i = 3, 4$), where n_i is the vibrational quantum number and l_i is the vibrational angular momentum. Following the classification by Boudon et al. (2006), we add the multiplicity index $M_i \leq L_i$ which we associate with the symmetry according with Table 2, where M_i is odd for F_i and F_2 and even for A_1, A_2, E. Imposing the condition $M_i \leq L_i$ automatically constrains $M_i = 0$ as A_1, $M_i = 1$ as F_2, $M_i = 2$ as E, and $M_i = 3$ as F_2. For higher values of M_i, these symmetry designations are repeated as shown in Table 2. We also choose $M_i = 6 + 12n$ for A_2 and $M_i = 12n$ for A_1. It should be noted however that for A_1 and A_2 these variations of M_i and L_i produce oversampled sets, and we choose the combinations with smallest M_i. It should be noted that the M quantum number introduced here caries additional information about the state symmetry in contrast to the multiplicity index C_i by Boudon et al. (2006).

The mapping between normal and local mode quantum numbers is built using the following rules:

$$\begin{aligned} v_1 + v_2 + v_3 + v_4 &= n_1 + n_3, \\ v_5 + v_6 &= n_2, \\ v_7 + v_8 + v_9 &= n_4 \end{aligned}$$

as well as using the relations between the vibrational symmetry $\Gamma_{\rm vib}$ (local mode label) of the vibrational basis functions $\Psi_i^{(J=0),\Gamma_{\rm vib}}$ and the vibrational angular momentum quantum numbers L_3, M_3, n_4, L_4, M_4 (normal mode labels) as explained above (see also Table 2). Each (local mode) vibrational basis functions $\Psi_i^{(J=0),\Gamma_{\rm vib}}$ is associated both with the normal and local mode quantum numbers, which are then propagated to the final ro-vibrational wavefunctions using the largest coefficient argument. The scheme appears to work well, at least it agrees with the conventional normal mode quantum numbers for the vibrational bands characterized experimentally. It is known, however, that for highly excited vibrational and rotational states characterized by strong mixing of the basis set components, the assignment based on the largest contribution $|C_i|^2$ from these

components may become meaningless. In order to keep track of the possible degradation of our assignment scheme, we retain the values of the corresponding largest coefficients $|C_i|^2$ in the Energy file, see Table 3.

Finally, we stress that our stretching vibrational basis set is not based on the harmonic oscillator functions. We use harmonic oscillators only as a reference to correlate the local mode quantum numbers with the conventional normal mode ones.

SUPPORTING INFORMATION

Additional Supporting Information may be found in the online version of this article:

Table 3. 10to10 Energy file.
Table 4. 10to10 Transition file.
(http://mnras.oxfordjournals.org/lookup/suppl/doi:10.1093/mnras/stu326/-/DC1).
Please note: Oxford University Press is not responsible for the content or functionality of any supporting materials supplied by the authors. Any queries (other than missing material) should be directed to the corresponding author for the article.

This paper has been typeset from a TEX/LATEX file prepared by the author.